Computer-Aided Design 192 (2026) 104029

Contents lists available at ScienceDirect

Computer-Aided Design

journal homepage: www.elsevier.com/locate/cad

Part orientation fused shape optimization for minimisation of print time and material waste in extrusion-based 3D printing

Don Pubudu Vishwana Joseph Jayakody [a,b,*], Bailin Deng [d], Ravindra S. Goonetilleke [e], Lauren E.J. Thomas-Seale [a,b], Hyunyoung Kim [c]

[a] Department of Mechanical Engineering, School of Engineering, University of Birmingham, Birmingham, B15 2TT, United Kingdom
[b] Topological Design Centre for Doctoral Training, University of Birmingham, Birmingham, B15 2TT, United Kingdom
[c] School of Computer Science, University of Birmingham, Birmingham, B15 2TT, United Kingdom
[d] School of Computer Science and Informatics, Cardiff University, Cardiff, United Kingdom
[e] Department of Management Science and Engineering, College of Engineering and Physical Sciences, Khalifa University, Abu Dhabi, 127788, United Arab Emirates

ARTICLE INFO

Keywords:
Shape optimization
Part orientation optimization
Design optimization
Sustainable design
Manufacturing-oriented design

ABSTRACT

Support structure generation is a critical requirement in additive manufacturing (AM) to prevent material collapse in overhanging regions. However, it increases print time, material waste, and overall production cost, especially in extrusion-based AM. To mitigate these problems, design engineers often resort to manually fine-tuning or even redesigning prototype geometry to minimise support structures, which is time-consuming and inefficient. A direct geometric optimisation that preserves locality of shape changes whilst corresponding to the part orientation remains an underdetermined problem.

In this paper, we present a novel alternating optimisation framework that finds the corresponding part geometry and orientation to minimise support structures under minimal geometric deviation. Whilst global-level support structure reduction is realised by the part orientation change, we introduce an efficient energy minimisation-based geometric optimisation framework, which is governed by saliency-aware elementwise projections and a set of manufacturing constraints. The proposed framework is validated through extensive computational and physical printing experiments employing multiple 3D printers and support structure types, on a diverse set of complex models including topologically non-trivial parts such as gyroid structures. Our results show an average reduction of 50 % in support structure print time, 27 % in material usage and 25 % in total print time, demonstrating the effectiveness of the proposed framework and its potential as a paradigm shift in manufacturing-oriented design.

1. Introduction

Material extrusion-based (i.e., Fused Deposition Modelling (FDM)) additive manufacturing (AM) is a highly flexible and cost-effective manufacturing method that converts digital 3D models to the physical form. The widespread availability of low-cost printer hardware has driven the successful commercialisation of FDM and has paved the way for numerous applications ranging from industry-grade part manufacturing to hobby-level rapid prototyping [1]. In standard commercial FDM 3D printers, the build (i.e., printing) direction is typically fixed. This constraint necessitates the generation of support structures to prevent the collapse of deposited material (along planar toolpaths), particularly in overhanging regions of the part geometry. Although essential, support structure generation significantly increases overall print time, leading to higher manufacturing related costs. Moreover, removal of support structures through post processing steps induces material wastage, deterioration of surface quality [2] in printed parts and additional labour expense, especially in industrial settings [1].

Therefore, minimising support structures remains a crucial challenge in AM-oriented design, with direct implications for efficiency, sustainability, and profitability. Design for AM (DfAM) methods such as part orientation optimisation [2,3] and support structure geometry optimisation [4,5] can be helpful in reducing the impact of support structure generation. Although such methods have already been integrated in

* Corresponding author at: postal address: Department of Mechanical Engineering, School of Engineering, University of Birmingham, Birmingham B15 2TT, United Kingdom.
E-mail address: dxj219@student.bham.ac.uk (D.P.V.J. Jayakody).

https://doi.org/10.1016/j.cad.2025.104029
Received 19 August 2025; Received in revised form 10 November 2025; Accepted 16 December 2025
Available online 17 December 2025

commercial slicing software programs, their effectiveness is highly diminished when processing complex parts that consist of high-genus (i.e., multiple through-hole) topology, large overhanging regions and highly curved features [4]. For most AM-based applications, design engineers are often faced with the challenge of fine-tuning the initial prototype geometry or even redesigning to reduce support structure requirements to maximise profits and performance (especially in mass manufacturing applications) [6]. This is a non-trivial and labour-intensive task that also demands expertise in manufacturing.

Although substantial deformation (i.e., global modification) of the part geometry is a possibility to achieve support structure reduction [7], it can be unsuitable for manufacturing-oriented design applications, and more importantly, inappropriate for topologically non-trivial (i.e., contain holes) complex geometries such as wireframe models or gyroid structures (see Fig. 1). Therefore, a generalised optimisation framework that minimises support structure dependency under minimal (i.e., local) geometric changes would be the desirable direction for most manufacturing oriented-design applications. On the other hand, the effect of part orientation on geometric optimisation has remained an underdetermined problem.

To the best of the authors' knowledge, the presented work is the first alternating optimisation framework that computes the optimal pair of part orientation and geometry to minimise support structures towards AM-oriented design optimisation. The core idea of the proposed alternating framework is to formulate a correspondence between part orientation and geometry, in contrast to conventional decoupled approaches. Whilst the global-level support structure volume reduction is governed by the part orientation change, an elementwise local projection-based method is introduced to locally optimise the corresponding geometry such that remaining overhang faces are converted into the overhang-free configuration. To ensure the adaptability for manufacturing oriented-design, our energy minimisation-based shape optimisation is formulated with a set of constraints to not only preserve salient (i.e., visually significant) features but also minimise distortions and deviation of the optimised geometry.

The proposed framework is efficient and directly operates on commonly used triangular mesh representations, which eliminates the bottleneck of conversion between volumetric mesh representations [7,8] for design optimisation. The effectiveness of the proposed framework is validated using extensive computational and physical printing experiments on a diverse set of 3D models, encompassing a wide range of complex geometric and topological features. To demonstrate the generalisability of our framework, we evaluate its performance under different support structure types using two FDM 3D printers along with their respective slicing software. The results demonstrate that on average, our framework realises reduction of support structure print time by 50 %, support material weight by 27 % and total print time by 25 % for selected groups of 3D models. In summary, the findings of this paper demonstrate that the alternating optimisation of part orientation and geometry is highly effective in minimising (in some cases, eliminating) support structures under minimal deviation from the original geometry and therefore can be crucial to improve the overall efficiency in extrusion-based additive manufacturing-oriented design applications.

1.1. Our contribution

The contributions of our work can be summarised as follows:

- A novel alternating part orientation and geometric optimisation framework to minimise support structure volume, thereby reducing material waste and print time in manufacturing-oriented design applications.
- An energy minimisation-based formulation combined with a saliency-aware elementwise projection and adaptive regularisation weighting scheme, enabling direct and efficient optimisation of triangle mesh geometry.
- Comprehensive validation of the generality and effectiveness of the framework through extensive computational and physical printing experiments using multiple FDM 3D printers, support structure types and slicing software, and a wide range of 3D models including topologically non-trivial complex geometries such as gyroid structures.

2. Related work

2.1. Freeform shape optimisation for 3D printing

Generally, the aim of shape optimisation is to find the optimal 'geometry' of a freeform 3D model that minimises (or maximises) a certain objective under a set of constraints. Whilst our work is focused on optimising the outer (i.e., boundary) geometry of freeform models, it is important to note that the internal geometry (e.g., lattice structure) [9] optimisation is a closely aligned notion to improve the standards of 3D printing. For example, several notable methods have focused on internal geometry optimisation to improve strength [9,10] and generate the desired elastic behaviour of 3D printed models [11,12]. On the other hand, Wang et al. [13] proposed a skin-frame geometric optimisation method to reduce the print volume and time of 3D printed objects.

In the domain of boundary shape optimisation, heuristic-based modelling (e.g., strut-adding and local thickening) [8], direct optimisation [14], and local optimisation [15] techniques have demonstrated that freeform part geometries can be optimised to improve structural strength of 3D printed models. Whilst the volumetric mesh-based method of Zhou et al. [14] induces excessive computational cost (e.g., more than 2 hours) for considerably simple 3D models, Musialski et al.

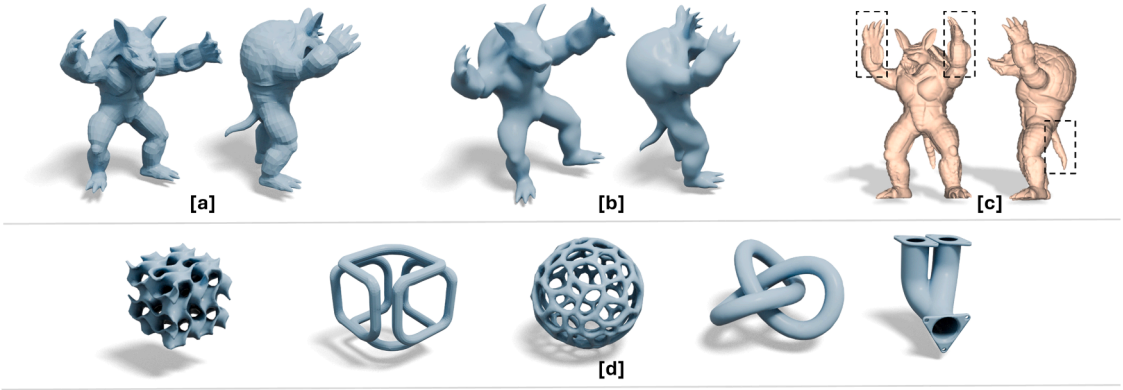

Fig. 1. Global vs. local geometric changes on topologically trivial and non-trivial models: (a). Original Armadillo model; (b). Optimised Armadillo model from our alternating optimisation framework; (c). Optimised Armadillo model from the method of Hu et al. [7] that applies large-scale (i.e., global) geometric changes; (d). Several topologically non-trivial models with complex geometric features inapplicable for global geometric changes.

[15] showed that a predominantly surface-based optimisation can be employed to achieve strength improvement whilst minimising computational costs. Similarly, the balance [16], buoyancy [15,17] and spinnability [18] of 3D printed parts can also be improved via the optimisation of freeform part geometry.

Jaiswal et al. [19] presented a geometric optimisation technique that operates on both global (i.e., boundary surface) and local (i.e., sliced layer boundary) levels to eliminate thin features to ensure printability. The framework of Hu et al. [7] showed that support structures can be reduced by large-scale deformation on topologically trivial (i.e., contains no holes) models. Whilst their method depends on a volumetric cage construction, the large-scale deformation-based (see Fig. 1(c)) optimisation can be infeasible for topologically non-trivial complex models (see Fig. 1(d)) which are often used in sensitive manufacturing-oriented design applications. In contrast to prior approaches, our work demonstrates that support structures can be minimised by directly optimising both topologically trivial and non-trivial geometries represented by boundary (triangle) meshes. Our energy minimisation-driven geometric optimisation (see Section 4.2) is generalisable to both topologically trivial and non-trivial complex geometries, enabling local and smooth geometric modifications to improve the manufacturability under minimal geometric deviation.

2.2. Part orientation optimisation for 3D printing

Part orientation optimisation has been well-studied as a means to improve the standards of FDM 3D printing [20]. For example, part orientation can be optimised to improve the surface quality [2] and structural strength [21,22] of 3D printed models. The computational methods presented by Wang et al. [23], Shi et al. [24] and Vanek et al. [4] showed that support structure minimisation can be realised by optimising the part orientation of freeform geometric models.

The influence of part orientation has also been integral in the context of geometric optimisation. For instance, Stava et al. [8] employed an upright part orientation selection [25] as a pre-processing step to improve that stability of 3D models, prior to the strength-based geometry modifications. Vanek et al. [4] employed part orientation selection as a pre-processing tool to minimise support inducing regions to improve the efficiency of optimising support structure geometry, which is in fact a function of part geometry. In contrast, Hu et al. [7] applied shape optimisation on a set of part orientation samples to find the best orientation candidate that minimises support structures.

In general, existing methods treat part orientation selection as a separate (i.e., decoupled) one-time step which can be suboptimal for optimising the part geometry for support structure reduction. Our work demonstrates that such a decoupled approach is less effective for support structure reduction, particularly when geometric changes must be minimal. Furthermore, brute-force techniques that optimise part geometry across a large set of orientation candidates [7] are computationally expensive and often impractical for manufacturing-oriented design applications. To address these limitations, we propose an alternating optimisation of part geometry and orientation to formulate the correspondence between the two entities, enabling the computation of the optimal pair of orientation and geometry that minimises support structure volume under minimal geometric deviation.

3. Overview and preleminaries

The input to our optimisation framework is a triangle mesh (i.e., a 2-manifold) M with $\mathbf{V} \in \mathbb{R}^{n\times 3}$vertices and $\mathbf{F} \in \mathbb{Z}^{m\times 3}$ faces. Our goal is to minimise the volume of support structures (Section 3.1) by optimising the part orientation $\theta \in SO(3)$ and geometry $\mathbf{V}$ whilst complying with a set of geometric constraints (e.g., minimal deviation, fixed regions) crucial for manufacturing-oriented design applications. To achieve this, we propose an alternating optimisation of $(\theta, \mathbf{V})$, which decomposes the complex problem of simultaneous optimisation into two simpler sub-problems (Section 3.2), and demonstrates robust performance across a wide range of complex geometries. The system pipeline of the proposed framework is depicted in Fig. 2.

3.1. Support structure volume

Note that different support structure geometry types (e.g., column, tree) can be generated in modern-day commercial slicing software programs. More importantly, direct computation of support structure volume can be realised by ray-based approaches [26] which distinguish between support structure columns that are directly connected to the build plate and those built on the part geometry. Whilst accurate, such methods are typically non-differentiable and computationally expensive (see Fig. 3), which makes them infeasible for iterative optimisation. To address this, we formulate an efficient proxy function to approximate the total support structure volume associated with the set of overhang faces $\{F_{ov}\} \subseteq \mathbf{F}$. Intuitively, for a given overhang face $f = (\mathbf{v}_1, \mathbf{v}_2, \mathbf{v}_3) \epsilon \{F_{ov}\}$, our proxy function aims to approximate the volume of the support column built beneath it (see Fig. 3). Let α_{max} denote the pre-defined critical angle (i.e., overhang angle threshold), between the normal vector of f, $\mathbf{n}_f$ and the build direction $\hat{\mathbf{z}}$ (see Fig. 3(a)). Note that the overhang angle $\cos\alpha = \mathbf{n}_f \cdot \hat{\mathbf{z}}$ of f satisfies the condition of $\cos\alpha < \cos\alpha_{max}$, where $|\cdot|$ denotes the dot product between two vectors. The total volume of the support structure columns that correspond to $\{F_{ov}\}$ can be approximated using our proxy function as below:

$$S_M(\theta, \mathbf{V}) = \frac{\sum_{f\epsilon\{F_{ov}\}} A_f \times \left|\mathbf{n}_f \cdot \hat{\mathbf{z}}\right| \times h_f}{|F_{ov}|} \tag{1}$$

where $A_f = \frac{1}{2} \parallel (\mathbf{v}_2 - \mathbf{v}_1) \times (\mathbf{v}_3 - \mathbf{v}_1) \parallel$ represents the area of f and h_f represents the height of the centroid $\mathbf{c}_f = \frac{1}{3}(\mathbf{v}_1 + \mathbf{v}_2 + \mathbf{v}_3)$ of f. Note that $A_f \times \left|\mathbf{n}_f \cdot \hat{\mathbf{z}}\right|$ corresponds to the projected face area on the ground plane (i.e., build plate). Compared to the ray-based support structure approximation [26] which can distinguish between the support structures built on the mesh faces (i.e., footing faces [27]) and the build plate, our projection-based approximation method offers a significant improvement in efficiency with sufficient accuracy (see Fig. 3).

3.2. Optimisation problem

Minimisation of support structure volume S_M can be generally described as minimising a function of two design variables as follows:

$$\min_{(\theta_n, \mathbf{V}_n) \in \theta \times \mathbf{V}} S_M(\theta_n, \mathbf{V}_n) \tag{2}$$

where $(\theta_n, \mathbf{V}_n)$ represents a corresponding pair of part orientation and vertex position matrix. To find an effective solution to the above problem, we adopt a well-known alternating optimisation approach [28] in which the minimisation is performed with one variable whilst the other is fixed (i.e., decomposes a given complex joint optimisation problem into simpler sub-problems that are easier to solve). For instance, given the initial (i.e., input) geometry $\mathbf{V}_{n(0)} \in \mathbf{V}$, the following sequence of minimisation problems can be solved iteratively to find the best orientation and geometry that minimises S_M as follows (see Algorithm 1):

$$\theta_{n(i)} \in \arg\min_{\theta_n \in \theta} S_M(\theta, \mathbf{V}_{n(i-1)}),\ i \geq 0 \tag{3}$$

$$\mathbf{V}_{n(i)} \in \arg\min_{\mathbf{V}_n \in \mathbf{V}} S_M(\theta_{n(i)}, \mathbf{V}) \tag{4}$$

Where i represents the iteration number. First, the part orientation optimisation defined in eq. (3) is solved globally using a direct sampling on the unit sphere S^2(see Section 4.1). We then propose an energy minimisation-based approach to realise local geometric optimisation defined in eq. (4), where the core idea is to minimise the proximity energy with respect to the projected geometry onto the saliency-aware overhang-free constraint space (see Section 4.2). In addition, our

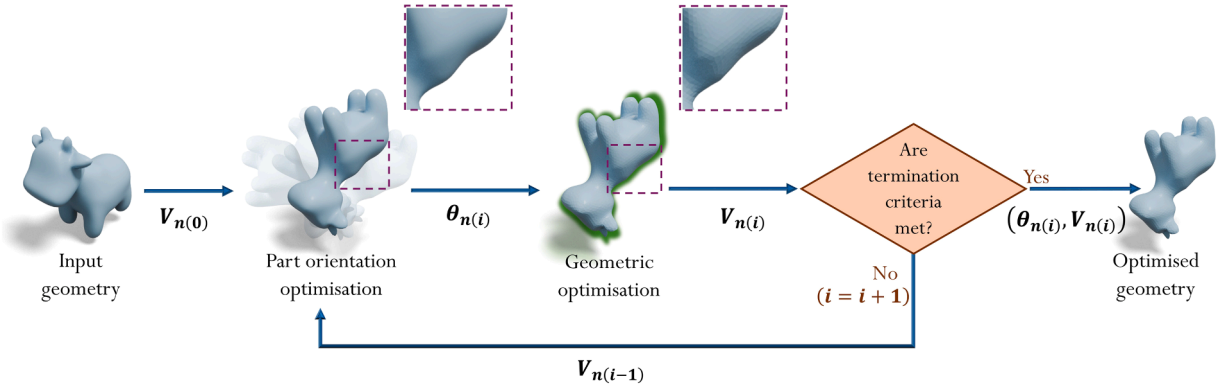

Fig. 2. The pipeline of our alternating optimisation of part orientation and geometry.

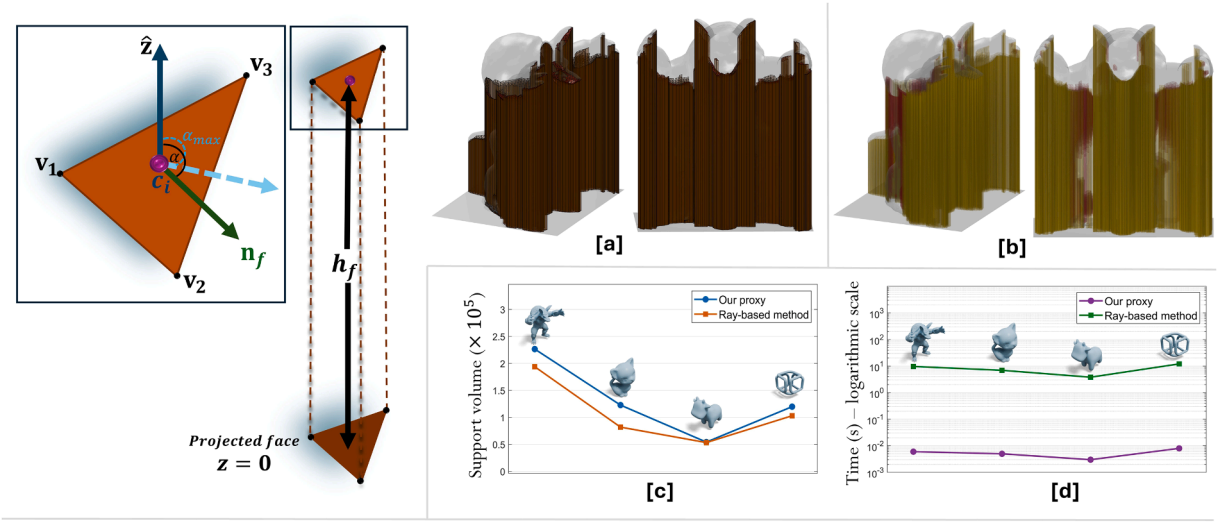

Fig. 3. Support structure volume approximation: (a). Our proxy function; (b). Ray-based approach similar to the concept proposed by Allaire et al. [26] that distinguishes between intersecting (red) and non-intersecting (yellow) support columns; (c). Difference between the approximated support structure volume from our method and the ray-based approach; (d). Computational time difference between our method and the ray-based approach.

geometric optimisation complies with a set of constraints to ensure that optimised geometry remains smooth and as close as possible to the original geometry, which are desirable qualities for many manufacturing-oriented design applications. Our alternating optimisation approach not only realises the correspondence between the part orientation and geometry but also enables support structure minimisation with minimal geometric deviation (see Section 5).

4. Part orientation fused shape optimisation

This section presents the detailed implementation of the complete alternating part geometry and orientation optimisation for support structure minimisation. Note that for parts which the orientation change is undesirable (or ineffective), our geometric optimisation (see Section 4.2) can be employed as a standalone method to minimise support structure volume whilst complying with deviation and distortion constraints.

4.1. Part orientation optimisation

Evidently, orientation of M has a global influence on the required support structure volume, especially for complex geometries. The optimality of part orientation must be well-defined to not only reduce support structure volume but also the number of faces attached to support structure columns $|F_{ov}|$, to ensure surface quality deterioration during support structure removal [2] is minimised (see Fig. 4). By modifying the Eq. (1), a proxy function that approximates the influence of support structure volume can be formulated as follows:

$$S_{prox}(\theta_{n(i)}) = w_1|F_{ov}| + w_2\frac{\sum_{f\epsilon F_{ov}} A_f \times |\mathbf{n}_f \cdot \hat{\mathbf{z}}| \times h_f}{|F_{ov}|} \tag{5}$$

where w_1 and w_2 are user-defined weights to control the effect of number of overhang (i.e., support structure linked) faces $|F_{ov}|$ and support structure volume, respectively. Note that $|F_{ov}|$ is non-smooth with respect to the design variable $\theta_{n(i)}$ and therefore, employing a gradient-based solver can be difficult. To overcome this, we optimise $S_{prox}(\theta_{n(i)})$ over a set of sampled orientations on the 2-sphere. We employ the Fibonacci sampling lattice concept [29] to generate uniformly distributed samples on the 2-sphere, which avoids the anisotropy inherent to commonly used random or grid-based Euler angle sampling methods. Let $\mathbf{d}_s = [x_s, y_s, z_s]$ denote a direction vector sampled on the unit sphere S^2 to represent the part orientation. Given a user-defined number $s = [1, 2, \ldots, N_d]$ of direction vector samples (see Fig. 5), the best part orientation $\mathbf{d}_{best}$ can be computed as:

$$\mathbf{d}_{best} = \underset{\mathbf{d}_s \in S^2}{argmin} S_{prox}(\mathbf{d}_s) \tag{6}$$

Algorithm 1
Alternating part orientation-fused shape optimisation.

Input: Initial mesh $M_o = (\mathbf{V}, \mathbf{F})$, Critical angle α_{max}, Fixed vertex indices F_x, Max alternating iterations N_a, Max orientation optimisation iterations N_b, Max shape optimisation iterations N_c, Orientation samples N_d, Termination criteria ϵ_{conv}, ϵ_{close}
Output: Optimised mesh $M^* = (\mathbf{V}^*, \mathbf{F})$

$\mathbf{s} =$ *ComputeMeshSaliency* $(\mathbf{V})$
Initialise vertex positions: $\mathbf{V}_{opt} \leftarrow \mathbf{V}$
$S_{M(best)} \leftarrow$*EstimateSupportStructureVolume* $(\mathbf{V}_{opt}, \mathbf{F}, \alpha_{max})$
$a \leftarrow 0, E_{dif} \leftarrow \infty, G_d \leftarrow 0$
while $(a \leq |N_a|)$ **and** $(E_{dif} \geq \epsilon_{conv})$ **and** $(G_d \leq \epsilon_{close})$ **do**
    //Step A: Global Orientation optimisation - Section 4.1
    $a \leftarrow a + 1$
    for $b \leftarrow 1$ **to** $|N_b|$ **do**
        $V_{temp}, S_{M(temp)} \leftarrow$*PartOrientationOptimisation* $(\mathbf{V}, \mathbf{F}, \alpha_{max}, N_d)$
        if $S_{M(temp)} < S_{M(best)}$ **then**
            $\mathbf{V}_{opt} \leftarrow \mathbf{V}_{temp}$,
            $S_{M(best)} \leftarrow S_{M(temp)}$
        end
    end
    //Step B: Shape optimisation - Section 4.2
    $\mathbf{V}, E_{dif}, G_d \leftarrow$*EnergyBasedShapeOptimisation* $(\mathbf{V}_{opt}, \mathbf{F}, \alpha_{max}, \mathbf{s}, F_x, N_c, \epsilon_{conv}, \epsilon_{close})$
end
$\mathbf{V}^* \leftarrow \mathbf{V}$
return $(\mathbf{V}^*, \mathbf{F})$

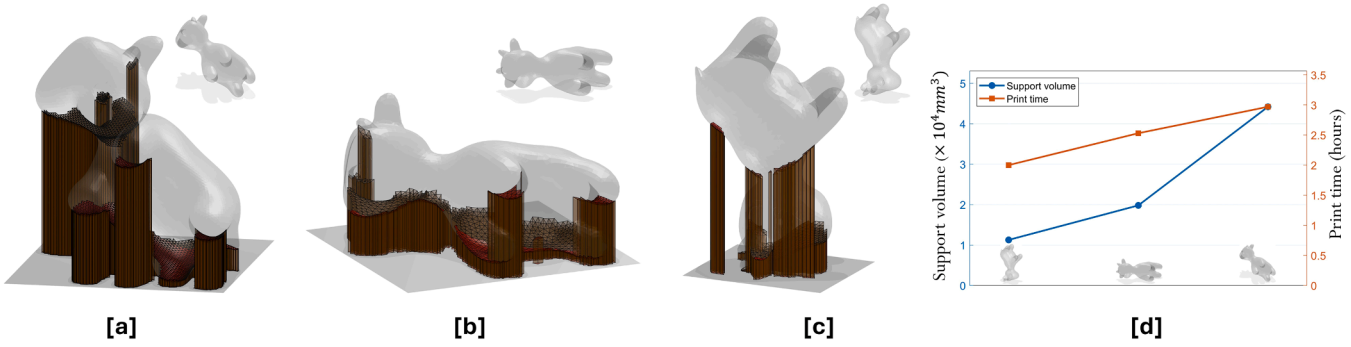

Fig. 4. Influence of the support structure proxy function towards the best orientation of the Spot model: (a). Part orientation generated by the CURA plugin Tweaker [3] causing large overhang region; (b). The orientation generated by the proxy defined in eq. (1); (c). The orientation generated by the proxy defined in eq. (5); (d). Comparison of the volume of generated support structure and the print time.

$$\mathbf{d}_s = \begin{bmatrix} x_s \\ y_s \\ z_s \end{bmatrix} = \begin{bmatrix} r_s \cos\alpha_g \\ 1 - \left[\frac{2s-1}{N_d}\right] \\ r_s \sin\alpha_g \end{bmatrix} \tag{7}$$

where $r_s = \sqrt{1 - {y_s}^2}$ represents the radius at y_s, and $\alpha_g = s.\ 2\pi\left[1 - \frac{1}{\varphi}\right]$ represents the golden angle derived from the golden ratio $\varphi = \frac{1+\sqrt{5}}{2} \approx 1.6$. It is important to note that the irrationality of the golden angle enables the uniform distribution of samples on the unit sphere [29]. Finally, vertices that correspond to the optimal orientation vector $\mathbf{d}_{best}$, $\mathbf{V}_B$, can be computed by the rotation matrix $\mathbf{R}_s$ as follows:

$$\mathbf{V}_B = \mathbf{V} \cdot {\mathbf{R}_s}^T \tag{8}$$

$$\mathbf{R}_s = \mathbf{I} + [\mathbf{a}_s]_\times \sin\theta_s + {[\mathbf{a}_s]_\times}^2 (1 - \cos\theta_s) \in SO(3) \tag{9}$$

Where $[\mathbf{a}_s]_\times = \begin{bmatrix} 0 & -a_{s,z} & a_{s,y} \\ a_{s,z} & 0 & -a_{s,x} \\ -a_{s,y} & a_{s,x} & 0 \end{bmatrix}$ represents the skew-symmetric matrix of the rotation axis $\mathbf{a}_s = \frac{\widehat{\mathbf{z}} \times \mathbf{d}_{best}}{\|\widehat{\mathbf{z}} \times \mathbf{d}_{best}\|}$, and $\theta_s = \arccos(\widehat{\mathbf{z}} \cdot \mathbf{d}_{best}) \in [0, \pi]$ represents the angle between $\mathbf{d}_{best}$ and the $\widehat{\mathbf{z}}$.

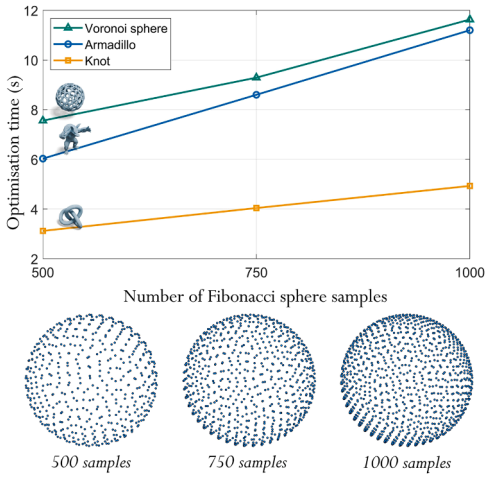

Fig. 5. Influence of the number of Fibonacci sphere samples N_d on the alternating optimisation time for several selected models – all models are tested with per-vertex deviation threshold $\epsilon_{close} = 0.005mm^2$.

4.2. Geometric optimisation

This section introduces our geometric optimisation which is formulated as an energy minimisation problem. From Section 4.2.1., we introduce the proximity energy term to minimise the elementwise deviation between the projected (i.e., target) shape. Next, a displacement smoothing energy term (Section 4.2.2) is included to ensure the optimised shape is smooth whilst minimising geometric distortion inherent to direct Laplacian smoothing [30]. Finally, the complete energy term and the required geometric constraints are introduced in Section 4.2.3.

4.2.1. Shape proximity energy

Our goal is a 'local' geometric optimisation that minimises support structure volume without global geometric changes (see Fig. 6). The core challenge in our case is to formulate an effective shape constraint that enables the conversion of each overhang face $f \in \{F_{ov}\}$ into overhang-free configuration, for which we employ the concept of local projection operators proposed by Bouaziz et al. [31]. For a given f with a face normal vector $\mathbf{n}_f$, the first step is to compute a new normal vector $\mathbf{n}_{proj}$ that projects f onto a new plane within the constraint space (i.e., an overhang-free plane that satisfies $\mathbf{n}_{proj} \cdot \hat{\mathbf{z}} < \cos\,\alpha_{max}$).Therefore, $\mathbf{n}_{proj}$ can be computed as:

$$\mathbf{n}' = \mathbf{n}_f - \left[\left(\mathbf{n}_f \cdot \hat{\mathbf{z}} - \cos\alpha_{max}\right)\hat{\mathbf{z}}\right] \tag{10}$$

$$\mathbf{n}_{proj} = \mathbf{n}' / \| \mathbf{n}' \| \tag{11}$$

Let f' denote the target face of a given f. For each vertex $\mathbf{v}_j \in \mathbb{R}^3$ of f, the orthogonal projection $\mathbf{y}_j$ onto the overhang-free plane defined by $\mathbf{n}_{proj}$ and the centroid of f, $\mathbf{c}_f = \frac{1}{3}(\mathbf{v}_1 + \mathbf{v}_2 + \mathbf{v}_3)$, can be computed as:

$$\mathbf{y}_j = \mathbf{v}_j - \left[\mathbf{n}_{proj} \cdot (\mathbf{v}_j - \mathbf{c}_f)\right]\mathbf{n}_{proj} \tag{12}$$

Once the target face coordinates $\{\mathbf{y}_j\}$ are known, the classical least-squares alignment [32] can be employed to perform the shape-preserving (i.e., distortion-free) elementwise projection $\mathbf{V}_{p*}$ from $\mathbf{v}_j$ onto $\{\mathbf{y}_j\}$ as:

$$\mathbf{V}_{p*} = \min_{\mathbf{R} \in SO(3)} \sum_j w_j \| (\mathbf{R}\mathbf{v}_j + \mathbf{t}) - \mathbf{y}_j \|^2 \tag{13}$$

where elementwise weighting $w_j = 1$ in our method. Note that the formulation in Eq. (13) yields rotation-aware vertex-level projections, which can be challenging to obtain through direct per-element rigid alignment [31]. Let $\mathbf{H} = \mathbf{V}_c^{\mathrm{T}} \mathbf{P} \mathbf{Y}_c$ denote the covariance matrix, where $\mathbf{P} = \mathbf{I}$ represents the diagonal weight matrix, and $\mathbf{V}_c$, $\mathbf{Y}_c$ represent the mean-centred coordinates of f and f', respectively. Then, the Singular Value Decomposition of $\mathbf{H}$, $SVD(\mathbf{H}) = \mathbf{U}\Sigma\mathbf{W}^{\mathbf{T}}$ can be used to find the rotation matrix $\mathbf{R}$ and translation $\mathbf{t}$ components of Eq. (13) as follows [32]:

$$\mathbf{R} = \mathbf{W}\mathbf{U}^{\mathbf{T}}, \mathbf{t} = \mathbf{c}_{f'} - \mathbf{R}\mathbf{c}_f \tag{14}$$

Where $\mathbf{c}_{f'}$ represents the centroidal coordinates of f'. However, since geometric change is governed by the vertex position changes, the elementwise projections $\mathbf{V}_{p*}$ must be converted into vertex-level whilst adhering to the local topology. Although averaging $\mathbf{V}_{p*}$ over the one-ring neighbourhood can be a straightforward solution, it is crucial that the induced geometric changes preserve salient features of M. In fact, our work proposes that the projections in 'overhanging salient regions' should be constrained to preserve the 'saliency'. Let $\mathbf{v}_M = \frac{1}{|F_B|}\sum_{f \in F_B} \mathbf{V}_{p*}(f) \mid F_B \subset \{F_{ov}\}$ denote the average of incident projected elements F_B, and $\boldsymbol{s} \in \mathbb{R}^{|\mathbf{V}| \times 1}$ denote the mesh saliency field proposed by Lee et al. [33]. The vertex-based saliency-aware projection for a given vertex $\mathbf{v}_j$ can be formulated as follows:

$$\mathbf{v}_j^{(p)} = (1 - s_j)\mathbf{v}_M + s_j \mathbf{v}_j^{(0)} \tag{15}$$

in which $s_j \in \boldsymbol{s}$ and $\mathbf{v}^{(0)}$ represent the vertex mesh saliency value and the original position of $\mathbf{v}$, respectively. Finally, for our constrained optimisation (see Section 4.2.3), the proximity energy term over the $\mathbf{V} \in \mathbb{R}^{n \times 3}$

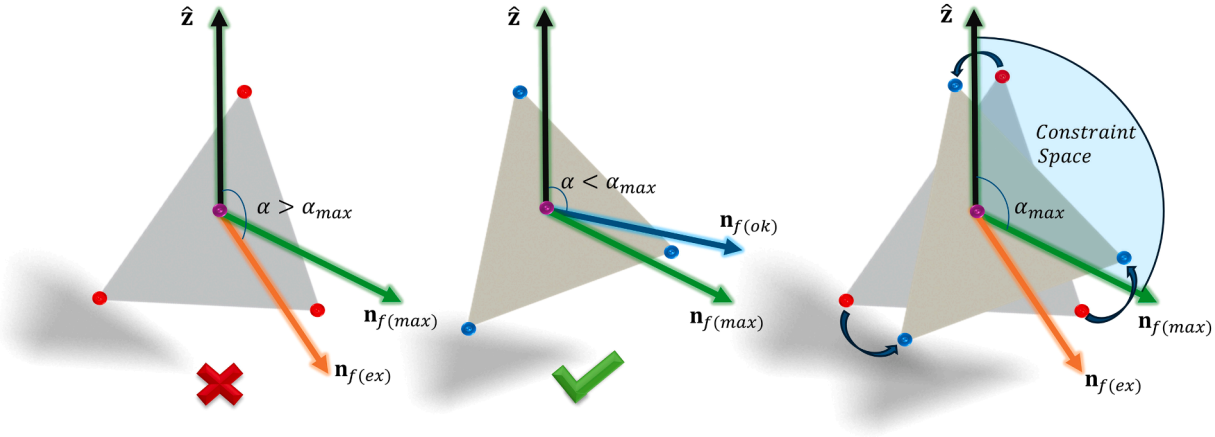

Fig. 6. The concept of elementwise projection: An overhang face (left) can be converted into an overhang-free configuration (middle) by the proposed least-squared local projection of faces into the overhang-free constraint space (right).

can be defined as:

$$E_p = \| \mathbf{V} - \mathbf{V}_{(P)} \|_F^2 \tag{16}$$

Where $\mathbf{V}_{(P)} \in \mathbb{R}^{n\times 3}$ represents the matrix of projected vertices and $\|\cdot\|_F$ denotes the Frobenius form.

4.2.2. Displacement smoothness and support volume energy terms

Smoothness of the geometry generated by above local projections is a crucial criterion in manufacturing-oriented design. Although Laplacian energy [31] is often used in geometry processing to enforce smoothness, it can potentially lead to large geometric deviation and shrinking and therefore, can be problematic towards our application. In addition, a direct geometric deviation penalisation with respect to the original geometry can over-constrain our optimisation problem. To provide a solution to these problems, we introduce the following displacement smoothness energy:

$$E_d = \| \mathbf{L}(\mathbf{V} - \mathbf{V}_{(0)}) \|_F^2 \tag{17}$$

where $\mathbf{L}$ represents the Laplacian matrix computed for $\mathbf{V}$, and $\mathbf{V}_{(0)}$ represents the original vertex positions. Next, although our local projection method is primarily focused on overhang face elimination, E_p is unaware of the support structure volume caused by the geometry. This can be problematic for practical shape optimisation applications. For instance, since a full projection of a given f into overhang-free plane is not feasible due to complying with other constraints (see Section 4.2.3) in most cases, a configuration that reduces the volume of the support structure column underneath f can be of great importance. To address this, we include a linear energy term E_S that directly penalises the support structure volume linked to $\mathbf{V}$ as:

$$E_s = \frac{\sum_{f\epsilon\ F_B} A_f \times \left|\mathbf{n}_f \cdot \hat{\mathbf{z}}\right| \times\ h_f}{|F_B| \times |F_{ov}|} \mid F_B \subset \{F_{ov}\} \tag{18}$$

where F_B represents the incident overhang faces. Note that the normalisation step with $|F_{ov}|$ is applied to limit the 'pull-down' force generated by the E_s.

4.2.3. The full energy-based optimisation and termination criteria

Our complete constrained shape optimisation problem can be formulated using the following total energy E:

$$\min\ E = \gamma \| \mathbf{V} - \mathbf{V}_{(P)} \|_F^2 + \beta \| \mathbf{L}(\mathbf{V} - \mathbf{V}_{(0)}) \|_F^2 + \mu E_S \tag{19}$$

s.t.

$$f \in F_x \rightarrow \mathbf{V} = \mathbf{V}_{(0)}$$

in which γ, β represent regularisation weights, and F_x represents the indices that correspond to fixed vertices defined by the user. A damping factor $\mu = 0.001$ is employed in our method to avoid degenerate cases caused by large influence of E_s on E. Note that E is predominately quadratic and by setting the $\nabla E = 0$, the system equation can be derived as follows:

$$\left(\gamma \mathbf{I} + \beta \mathbf{L}^{\mathrm{T}}\mathbf{L}\right)\mathbf{V} = \gamma \mathbf{V}_{(P)} + \beta \mathbf{L}^{\mathrm{T}}\mathbf{L}\mathbf{V}_{(0)} - 1/2 \begin{pmatrix} 0 \\ 0 \\ \mu E_S \end{pmatrix} \tag{20}$$

The selection of regularisation weights γ, β can have a significant influence on the shape optimisation process and can be challenging for novice users. More importantly, based on our experiments, the regularisation weights require fine-tuning for each tested part through repetitive simulations, causing an exhaustive and labour-intensive process. To avoid this problem, we propose an (optional) adaptive weight computation based on the iteration number c as follows:

$$\gamma = \mu_{proj} \times \exp(-k_1 c) \tag{21}$$

$$\beta = \mu_{smooth} \times (1 - \exp(-k_2 c)) \tag{22}$$

where μ_{proj} and μ_{smooth} are parameters that can be set by the user to control the 'scale' of influence of E_p and E_d. Therefore, as the optimisation progresses, β gradually increases smoothness whilst γ reduces the influence of projection, resulting in a natural shape change (see Figs. 7 and 8). Although the growth and decay rates k_1, k_2 have been fixed ($k_1 = 0.05$, $k_2 = 2 \times 10^{-6}$) in all our experiments, users can opt to change these values based on the nature of their applications. Note that $\mathbf{A} = \gamma \mathbf{I} + \beta \mathbf{L}^{\mathrm{T}}\mathbf{L}$ is a sparse and square matrix whilst fixed vertex constraints compromise its symmetry. The optimisation problem defined in eq. (20) can be efficiently solved using LU decomposition (see Section 5.1).

4.2.3.1. Termination criteria. To avoid degenerate cases (i.e., mesh collapse) and provide effective user control, several termination criteria are defined for the iterative process. First, a user-defined threshold ϵ_{close} is set to control the mean squared per-vertex geometric deviation G_d from the initial geometry $\mathbf{V}_{(0)}$ as follows:

$$G_d = 1/|V| \| \mathbf{V} - \mathbf{V}_{(0)} \|_F^2 > \epsilon_{close} \tag{23}$$

In addition, another user-defined threshold ϵ_{conv} is employed to terminate based on the energy difference (i.e., $E_{current} - E_{previous}$) in subsequent iterations as:

$$E_{dif} = E_{current} - E_{previous} < \epsilon_{conv} \tag{24}$$

5. Results and discussion

5.1. Implementation

The complete alternating opti+misation framework is implemented in MATLAB (MathWorks) on a laptop with an Intel(R) Core ™ i7 -12850HX CPU (2.1 GHz) + 32 GB RAM, running on Windows 10. Note that both Stereolithography (i.e., STL) or Wavefront Object (i.e., OBJ) mesh models can be provided as the input. We test our method on a range of models with complex geometric and topological features (see Figs.8 and 9). Note that the optimisation problem defined in Eq. (20) is solved by the MATLAB's mldivide operator \ which generally employs the LU decomposition method for sparse and square matrices similar to the $\mathbf{A} = \gamma \mathbf{I} + \beta \mathbf{L}^{\mathrm{T}}\mathbf{L}$.

The physical printing tests are carried out using two FDM 3D printers: Ultimaker S5 and Bambu X1 Carbon (see Fig. 10). CURA (Version 5.8.1) and Bambu Lab (Version 2.0.2.57) slicing software programs are used to generate the G-codes for Ultimaker S5 and Bambu X1 Carbon, respectively. The critical angle for support generation is set to 60°, in both slicing software programs. Polylactic Acid (PLA) material is used in both printers. As shown in Fig. 9, we compare the effectiveness of the proposed approach using two available support structure types in the slicing software: tree type and normal type (i.e., column structure type which is relevant to our support volume approximation). Note that, layer height is set to 0.2mm and infill percentage is set to 10 % (for fast printing) in both slicing programs for all the printing experiments. The source code of our complete optimisation framework will be released upon the acceptance of the paper.

5.2. Computational results

Table 1 presents the computational statistics of our complete alternating optimisation framework for a set of freeform models that exhibit both complex geometric and topological features. Note that the print time and material weight information of Table 1 are obtained from the CURA slicing software (for Armadillo, Spot, Knot) and Bambu Lab slicing software (for Voronoi sphere), and the alternating optimisation was run with Fibonacci sphere sampling of $N_d = 1000$ for all models. Our alternating optimisation method's runtime is under 12 seconds for

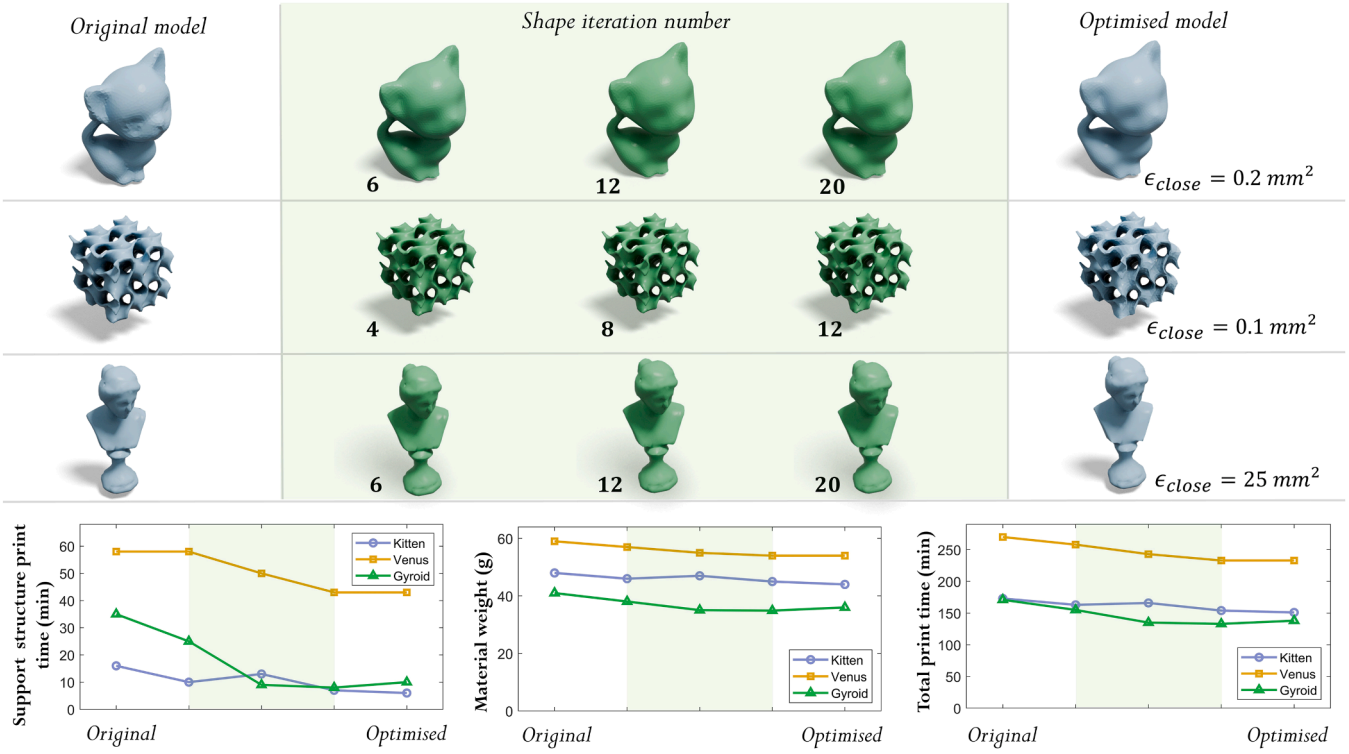

Fig. 7. Smooth transformation from original geometry to optimised geometry with different per-vertex deviation ϵ_{close} settings for Kitten, Gyroid structure and Venus models (top to bottom), and the comparison of support time, material weight and print time with respect to shape changes.

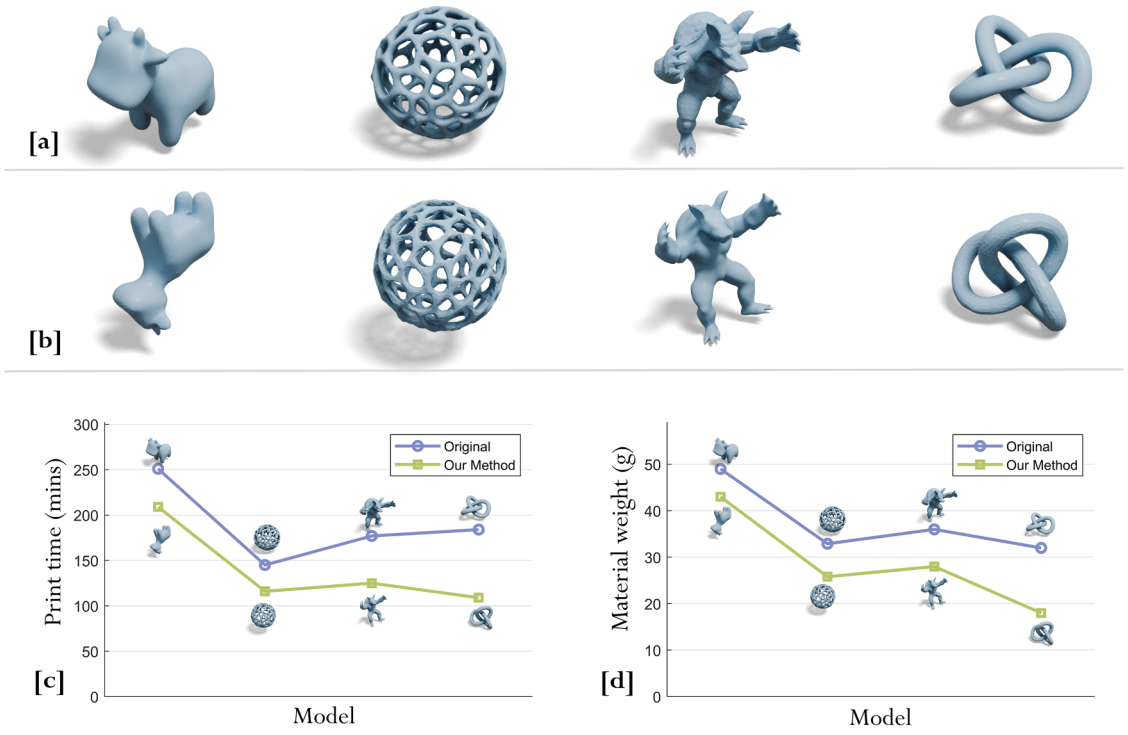

Fig. 8. Effectiveness in reducing print time and material weight by the proposed alternating optimisation method: (a). Original models; (b). Optimised models from the full alternating method; (c). Print time comparison; (d). Material weight comparison – All the statistics are obtained from the CURA slicer. Armadillo and Voronoi Sphere are sliced with tree support structures whilst Spot and Knot models are sliced with normal support structures.

all the tested models and reduces (on average) total print time and material weight by 24.95 % and 26.73 %, respectively (see Table 1). Note that although having a higher value for ϵ_{close} provides a larger design space for the geometric optimisation phase (see Fig. 11), it is not always proportional to the reduction of support structure or print time. For example, as shown in Fig. 12, support structure print time reduction

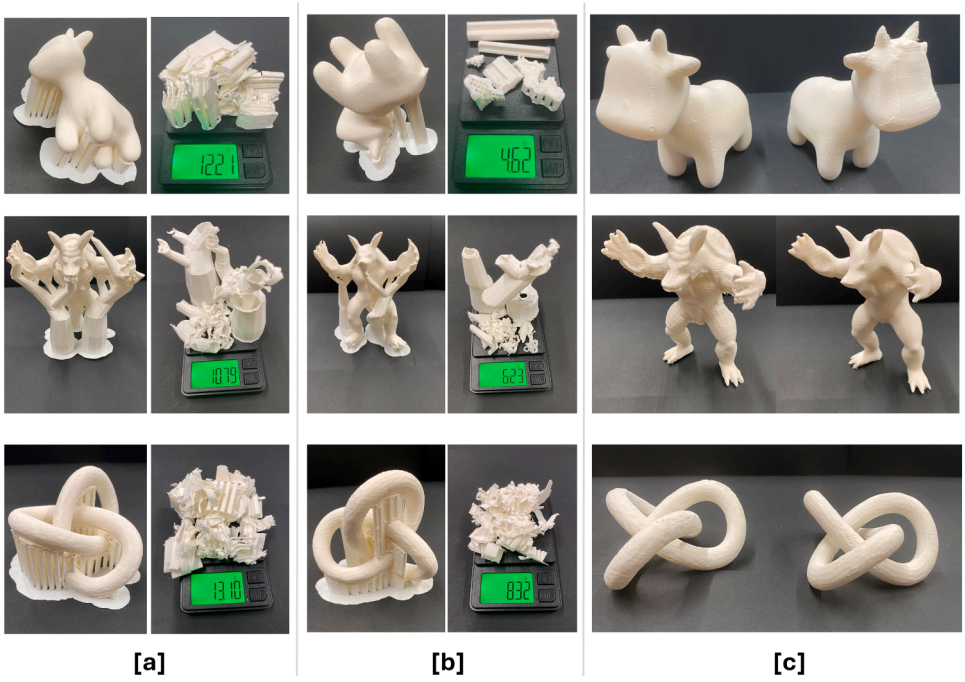

Fig. 9. Comparison between the printed original models and optimised models using our alternating optimisation framework (for Spot, Armadillo and Knot models): (a). Printed original models and their support structure weight – Spot and Knot models are oriented using tweaker plugin [3]; (b). Optimised models from our method and their support structure weight; (c). Visual comparison of original (left) and optimised (right) models.

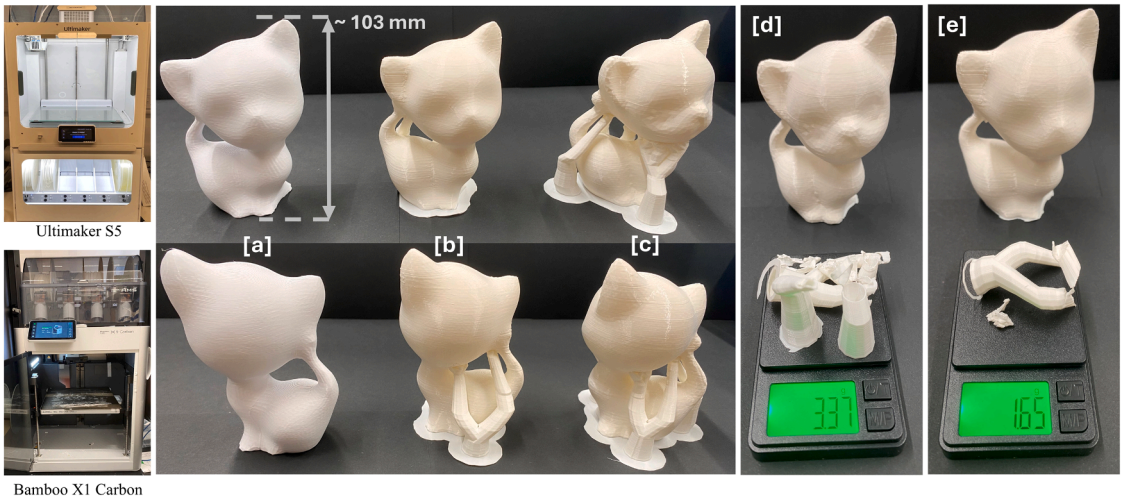

Fig. 10. Geometry optimisation towards support-free 3D printing (Kitten model): (a). Support-free printed optimised model ($\epsilon_{close} = 0.2mm^2$) using Bambu X1 carbon printer; (b-c). Optimised ($\epsilon_{close} = 0.2mm^2$) and original models printed using the Ultimaker S5 printer; (d). Support structure weight of the printed original model; (e). Support structure weight of the optimised model.

patterns with respect to the changes in per-vertex geometric deviation threshold ϵ_{close} can be different from one part to the other.

From Table 2, we present the results of the geometric optimisation (Section 4.2) as a standalone method to show its effectiveness in reducing support structure and print time. We set the ϵ_{close} within an appropriate range based on the scale of the mesh to avoid degenerate cases and extensive geometric feature loss. As shown in Fig. 13, our method is successful in optimising complex geometries such as gyroid structures to achieve a significant reduction of support structures and print time, whilst ensuring minimal deviation (i.e., $\epsilon_{close} = 0.1$) and maintaining fixed boundary regions. Note that some support structures remain inaccessible in the printed original gyroid structure. The geometry-only optimised Gyroid structure with its preserved boundary (see Fig. 13 (d)) not only eliminates such inaccessible support structures but also demonstrates the applicability of our geometric optimisation framework towards manufacturability-aware weight reduction for high-value manufacturing applications.

In both our alternating and geometry-only optimisation experiments, the overhang angle threshold α_{max} is set to 120°. To show the effect of changing α_{max}, we perform geometry-only optimisation on the Kitten model with different values for α_{max} and a fixed ϵ_{close} to ensure fair comparison. Evidently, reducing the threshold angle increases the number of overhang faces, resulting in a larger design space (i.e., higher total energy) which can be beneficial to achieve better overall performance (see Fig. 11 (e)). Regardless of ϵ_{close} and α_{max}, as shown in Fig. 14, our framework achieves monotonic minimisation of the total energy

Table 1
Computational statistics for alternating optimisation.

Model	Vertices	Original model		Optimised model – alternating optimisation method					
		Material (g)	Total print time (min)	Material (g)	Total print time (min)	Optimisation time	Deviation ϵ_{close} (mm^2)	Reduced material weight %	Reduced total print time %
Armadillo[†]	6719	49	251	43	209	11.201	0.01	16.7 %	12.2 %
Voronoi Sphere[†◇]	6513	32.9	145	25.8	116	11.636	0.005	20 %	21.6 %
Spot[†*]	4313	36	177	28	125	7.602	0.005	29.4 %	22.2 %
Knot[†*]	2532	32	184	18	109	4.763	0.005	40.8 %	43.8 %

[†] Sliced and printed with normal support structure type.
[‡] Sliced and printed with tree support structure type.
[*] Oriented using the tweaker [3] CURA slicer plugin.
[◇] Sliced from Bambu Lab slicer software

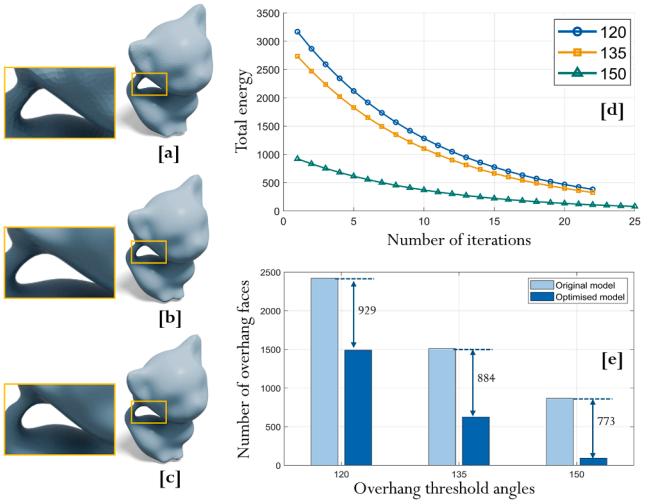

Fig. 11. Influence of the overhang angle threshold α_{max} on the total energy and shape (Kitten model) with a fixed ϵ_{close}: (a). Optimised model with $\alpha_{max} = 120°$; (b). Optimised model with $\alpha_{max} = 135°$; (c). Optimised model with $\alpha_{max} = 150°$; (d). Total energy levels; (e). Comparison of the number of overhanging faces of before and after optimisation for each threshold level.

defined in Eq. (19).

To further validate the effectiveness of our method, we compare the (estimated) support structure print times obtained from CURA slicer software. Several testcases of geometry-only and alternating optimisation are selected for this comparison and as shown in Table 3, the optimised models reduce support structure print time by 50.02 % on average. In general, our complete alternating method achieves better performance (i.e., reducing more support structures under lower ϵ_{close}) compared to the geometry-only optimisation approach. To further highlight the advantage of our alternating optimisation, we provide a comparison with geometry-only and orientation-only optimisation [3] for three different models in Table 4. It is evident that both geometry-only and alternating optimisation outperform orientation-only optimisation for all the tested models. For Knot and Spot models, our alternating method achieves greater print time reduction while maintaining lower geometric deviation compared to the geometry-only approach (see Table 4).

Although allowing a higher ϵ_{close} can lead to higher support structure reduction through geometry-only optimisation, minimising geometric deviation can be of great importance for manufacturing complex models with thin features. For instance, as shown in Table 4, geometry-only optimisation reduces more print time than the alternating method at the cost of a greater geometric deviation. Another example illustrating this insight is the comparison between the geometry-only optimisation (with a higher ϵ_{close} value) and the alternating optimisation of the

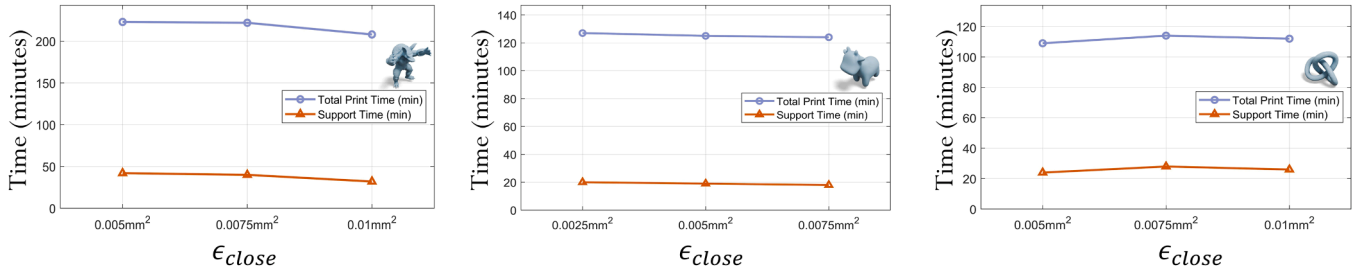

Fig. 12. Influence of the per-vertex deviation threshold ϵ_{close} on the total print time and support print time for several models optimised with our alternating method: Armadillo (left), Spot (middle) and Knot (right).

Table 2
Computational statistics for Geometry-only optimisation.

Model	Vertices	Original model		Geometry-only optimised model					
		Material (g)	Total print time (min)	Material (g)	Total print time (min)	Optimisation time	Deviation ϵ_{close} (mm^2)	Reduced material weight %	Reduced total print time %
Gyroid[◇]	10431	41	171	36	138	6.712	0.1	12.2 %	19.3 %
Kitten	5569	48	173	44	151	4.773	0.2	8.3 %	12.7 %
Cube	7037	38	204	32	185	5.513	0.25	15.8 %	9.3 %
Venus	1397	59	270	54	233	0.685	25	8.5 %	13.7 %

[◇] Sliced from Bambu Lab slicer software

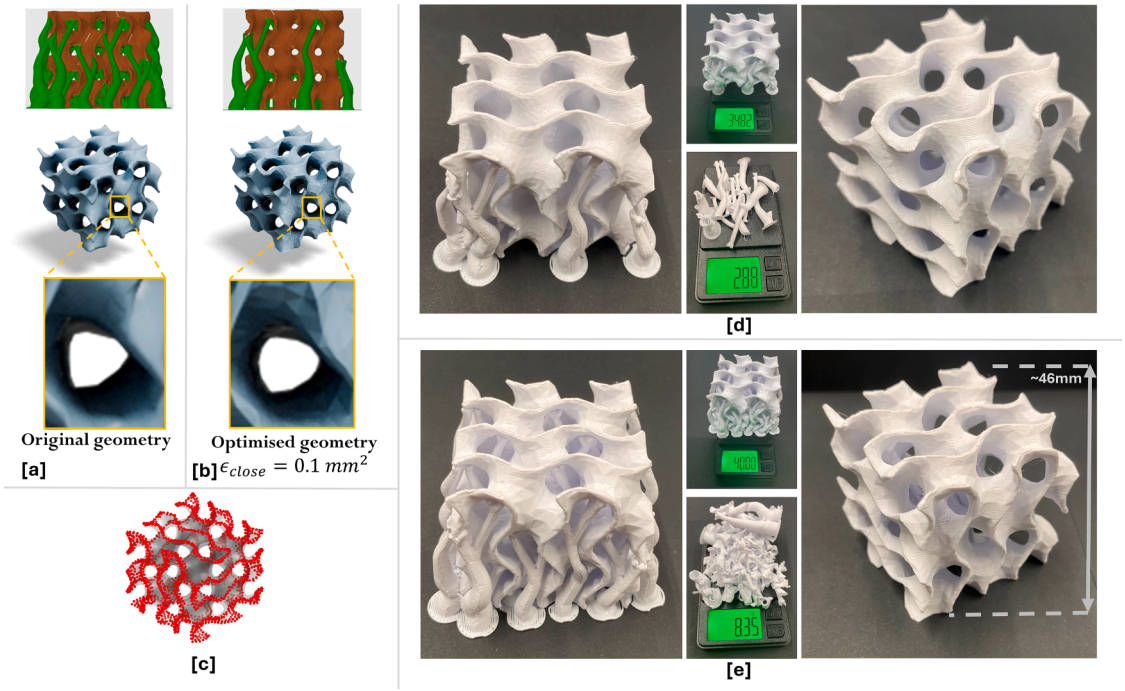

Fig. 13. Geometry-only optimisation of internal structures (Gyroid model): (a). Original gyroid structure and the sliced result on Bambu slicer software; (b). Optimised gyroid structure and the sliced result; (c). Fixed regions; (d). Printed optimised gyroid structure and the weight of its support structure using the Bambu X1 Carbon printer; (e). Printed original gyroid structure and the weight of a portion of its support structure (note several support structures are left in inaccessible regions).

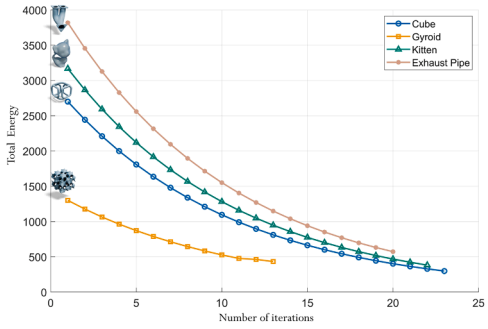

Fig. 14. Total energy E levels during geometry optimisation of several test models with different ϵ_{close} values.

Table 3
Support structure print time comparison.

Model	Original model – Support structure print time◊ (min)	Optimised model			
		Optimisation method		Support structure print time (min)	Reduced support structure print time %
		Alternating	Geometry-only		
Kitten	16		√	06	62.5 %
Cube	44		√	38	13.6 %
Knot†	63	√		24	62.4 %
Armadillo	58	√		32	44.9 %
Spot	57	√		19	66.7 %

† Sliced and printed with normal support structure type.
◊ Estimated from CURA slicer software

Voronoi sphere in Fig. 15. Evidently, geometry-only optimisation of Voronoi sphere reduces more support structures (and print time) under large geometric deviation that leads to local thin features (see Fig. 15 (f)). In contrast, our alternating optimisation realises significant reduction of print time and support structures compared to the original model with minimal geometric deviation and no thin features, which can be the ideal solution for such topologically complex geometries.

5.2.1. Salient feature preservation

Our salient feature-aware vertex projection aims to limit the geometric deviation in 'overhanging salient regions'. To demonstrate the effectiveness of the proposed approach, we first compute the vertex displacements $d_{NS} = \| \mathbf{v}_j^{(p)} - \mathbf{v}_j^{(0)} \|^2$ from our proposed salient feature-aware projection for the geometry-only optimisation of Kitten model.

Let $\mathbf{v}_j^{(ap)} = \frac{1}{|F_B|} \sum_{f \epsilon F_B} \mathbf{V}_{p*}(f)$ denote the average projection of incident face elements of a vertex $\mathbf{v}_j$. By replacing $\mathbf{v}_j^{(p)}$ with $\mathbf{v}_j^{(ap)}$, we run the geometry-only optimisation for the Kitten model and recompute the vertex displacements as $d_S = \| \mathbf{v}_j^{(ap)} - \mathbf{v}_j^{(0)} \|^2$. Then, to visualise the difference between the two projection methods, a scalar field map δ can be computed as follows:

$$\delta = d_{NS} - d_S \tag{25}$$

As shown Fig. 16, higher δ values can be observed in regions where large areas of salient but overhanging (i.e., critical) features exist, which demonstrates the effectiveness of the proposed saliency-aware vertex projection over the average projection method.

5.3. Physical validation of 3D printed models

First, as shown in Fig. 9, we print the original models and optimised models from our complete alternating method to validate the performance. Furthermore, to verify the statistics of the performance on support structure reduction (see Table 3), we measure the weight of removed support structures on a mini scale with a weight range from 0.01-1000g, for both original and optimised models. To show the applicability of our method under different support structures, we employ both tree-type and normal-type support structures for physical

Table 4
Comparison of total print time for different optimisation methods.

Model	Original model -Total print time (min)	Optimisation method						
		Orientation-only*		Geometry-only ($\epsilon_{close} = 0.1mm^2$)		Alternating (part orientation and geometry)		
		Total print time (min)	Reduced total print time %	Total print time (min)	Reduced total print time %	Deviation ϵ_{close} (mm^2)	Total print time (min)	Reduced total print time %
Armadillo‡	251	228	9.16 %	211	15.94 %	0.01	224	10.76 %
Spot†	177	175	0 %	152	8.43 %	0.005	143	13.86 %
Knot†	166	190	1.13 %	156	11.86 %	0.005	125	29.38 %

† Sliced and printed with normal support structure type.
‡ Sliced and printed with tree support structure type.
* Orientation optimisation is performed by the tweaker [3] CURA slicer plugin.

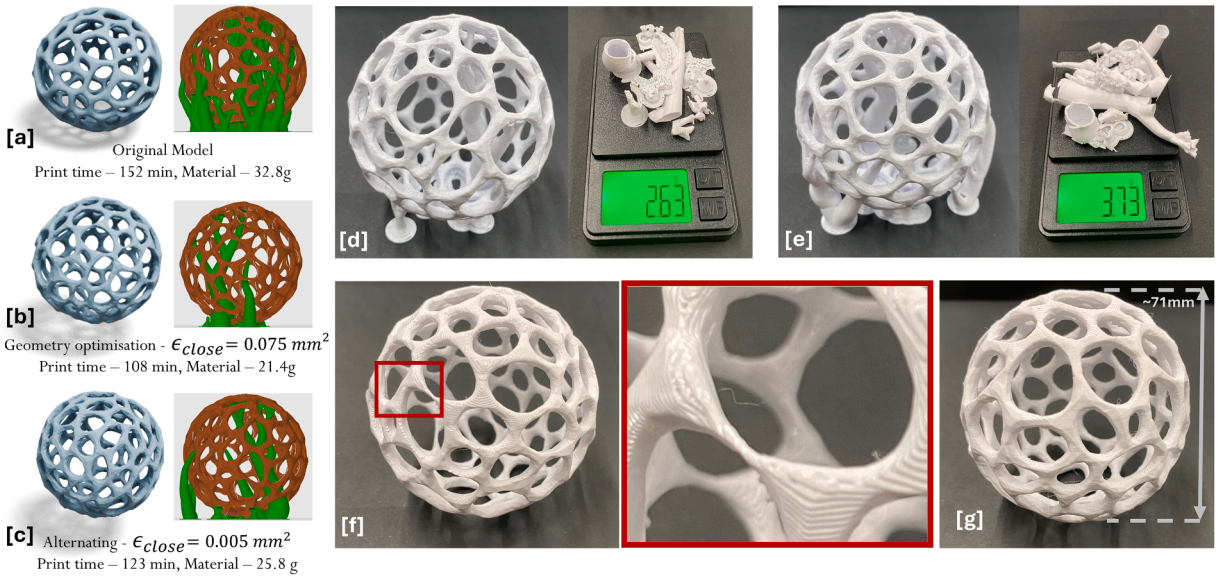

Fig. 15. Results for the Voronoi sphere model: (a-c). Geometry and the sliced results (from Bambu Lab) of the original, geometry-only optimised and alternating optimised models; (d). Printed geometry-only optimised model; (e). Printed alternating optimised model; (f). Support-removed geometry-only optimised model; (g). Support-removed alternating optimised model.

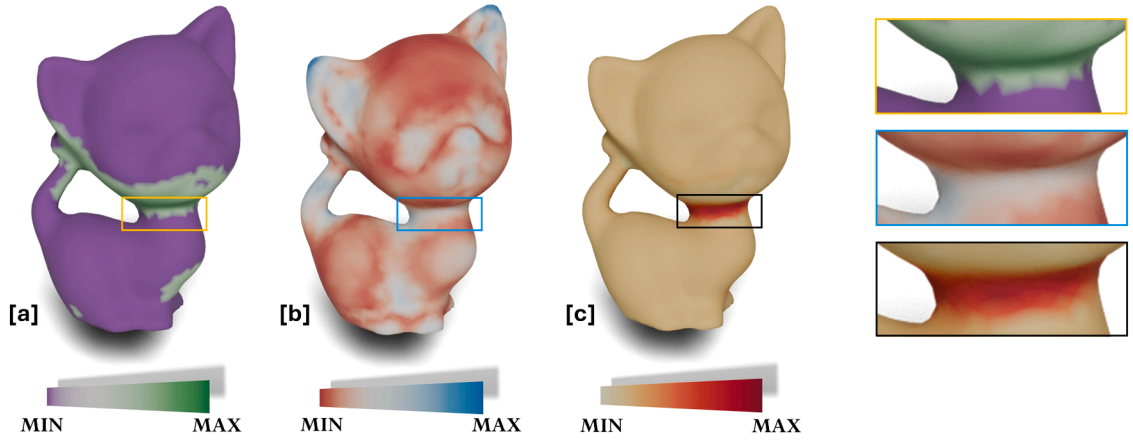

Fig. 16. Effect of our saliency-aware elementwise projection towards salient feature preservation (Kitten model): (a). Overhang scalar field; (b). Mesh saliency scalar field [33]; (c). Scalar map δ that depicts the difference between vertex displacements caused by average projection and our salient-aware projection.

printing experiments (see Fig. 9). Note that for a given model, the amount of support structures required for overhanging regions defined by a maximal critical angle α_{max} can vary based on the 3D printer hardware [34]. For instance, as shown in Fig. 10, given the identical support structure generation software settings and ϵ_{close}, the geometry-only optimised Kitten model which requires a small amount of support structures on the Ultimaker S5 can be printed without any support on the Bambu X1 Carbon.

5.3.1. *Optimised models from the alternating method*

Several test models (Spot, Armadillo, Knot) of our alternating method are printed using Ultimaker S5 and as shown in Fig. 9, a

significant difference of support structure weight can be observed between the original and optimised models. The Voronoi sphere model optimised by our alternating method is printed on the Bambu X1 Carbon printer. In general, our alternating method realises significant savings of print time and material for all the tested models. Note that the tweaker plugin's [3] algorithm is purely driven by support structure volume reduction whilst constraining base patch size, which can be suboptimal in many cases (see Fig. 9). In contrast, our part orientation optimisation phase focuses on reducing both support volume and the number of overhang faces (i.e., linkages to support structure columns). As a result, our alternating optimisation has higher performance compared to the oriented models using the tweaker plugin (see Fig. 9) which are prone to large overhanging regions, leading to high surface quality damage.

5.3.2. Geometry-only optimised models

As shown in Fig. 10, our geometry-only optimisation is effective in elimination (on Bambu X1 Carbon) or minimisation (on Ultimaker S5) of support structures whilst minimising deviation and preserving salient features (see Fig. 16) for topologically trivial models such as Kitten. Note that although saliency feature preservation is effective, it can be compromised on certain (especially smaller or inconsistently salient but constrained) regions to comply with other constraints of our optimisation (see Fig. 16(c)). As a solution, users can opt for the complete fixation of important regions, similar to the geometric-only optimisation of the Venus model depicted in Fig. 17. Note that the sliced results of the Venus model (see Fig. 17 (f-g)) demonstrate that our method is valid for both tree and normal support structure types. Similar to the performance on topologically non-trivial complex geometries such as gyroid structure (Fig. 13) and Voronoi sphere (Fig. 15), our method realises notable savings of manufacturing costs for the complex cube model (see Fig. 18), under minimal geometric deviation from the original geometry. From Fig. 19, we show the geometric optimisation result of the complex geometry of exhaust pipe which also contains non-trivial topological features. We fix both functional and critical regions of the exhaust pipe geometry and optimise it with a deviation of $\epsilon_{close} = 0.1$. As the support structures are generated internally (i.e., inaccessible) and externally for both the original and optimised models, we compare the total weight of the geometry and support structures. As shown in Fig. 19, our method realises a considerable reduction of total weight by minimising support structures under heavy constraints, which shows the potential of our method for cost-cutting in mass manufacturing of mechanical parts. In similar instances where the internal support structure elimination is impossible (e.g., exhaust pipe), using a soluble material (e.g., Polyvinyl Alcohol (PVA)) can be more desirable for the purpose of printing support structures.

5.4. Limitations and future work

5.4.1. Geometric optimisation-related limitations

Both our alternating and geometry-only optimisation methods realise significant reduction of print time and material waste for a range of complex models. Specifically, the manufacturability of complex topologically non-trivial models with fewer (or no) sharp geometric features (e.g., Voronoi sphere, gyroid) can be significantly improved whilst guaranteeing locality of shape changes. However, allowing large ϵ_{close} to improve the manufacturability can induce sharp feature losses for models such as Kitten (see Fig. 10). As shown in Fig. 17, this drawback can be alleviated by fixing (i.e., constraining displacements) large regions with sharp features (e.g., the face of Venus) or restricting the ϵ_{close} to the minimum, with a trade-off in the performance of support structure reduction. We remark that having low values for both ϵ_{close} and α_{max} can result in an ill- constrained system. In addition, for functional interfacing parts (e.g., Exhaust pipe in Fig. 19) in applications such as assemblies, the interfacing regions must be fixed prior to geometric optimisation in our current framework, restricting the potential for broader shape exploration.

Since our geometric optimisation involves rigid rotation of face elements, faces that correspond to flat base regions of models such as Kitten must be fixed to avoid undesirable changes to the surrounding geometry (e.g., sharp dents which move below the ground plane). Next, although our displacement smoothing energy term provides a solution to simultaneously maintain smoothness of optimised geometry and proximity to the original geometry, it can be prone to surface feature distortion. Whilst the regularisation weights (i.e., μ_{proj} and μ_{smooth}) remain fixed in our current implementation, finetuning them for specific design applications can be an option to reduce the distortions inherent to both the elementwise projection operation and displacement smoothing term. On the other hand, integration of feature preserving smoothing techniques [35] can be useful to minimise the surface feature distortions.

It is important to note that our current implementation depends on the mesh quality and can be ineffective for large high-quality meshes or highly irregular meshes. Therefore, it would be interesting to experiment with fast rotational alignment methods [36] and optimisation accelerating schemes similar to the work proposed by Peng et al. [37], to investigate the feasibility of directly processing high quality meshes. In

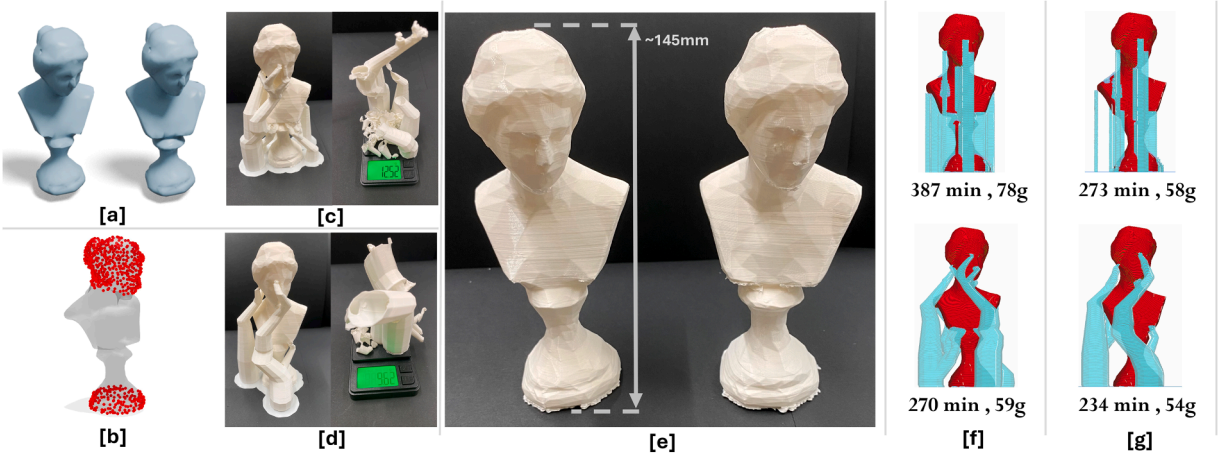

Fig. 17. Results for the Venus model (geometry-only optimisation): (a). Optimised (left) and original (right) models; (b). Fixed regions (depicted in red); (c). Printed original model and weight of the support structure; (d). Printed optimised model and weight of the support structure; (e). Support-removed printed optimised (left) and original (right) models; (f). Normal (top) and tree (bottom) support structure generated on CURA slicer for the original model; (g). Normal (top) and tree (bottom) support structure generated using the CURA slicer software for the optimised model.

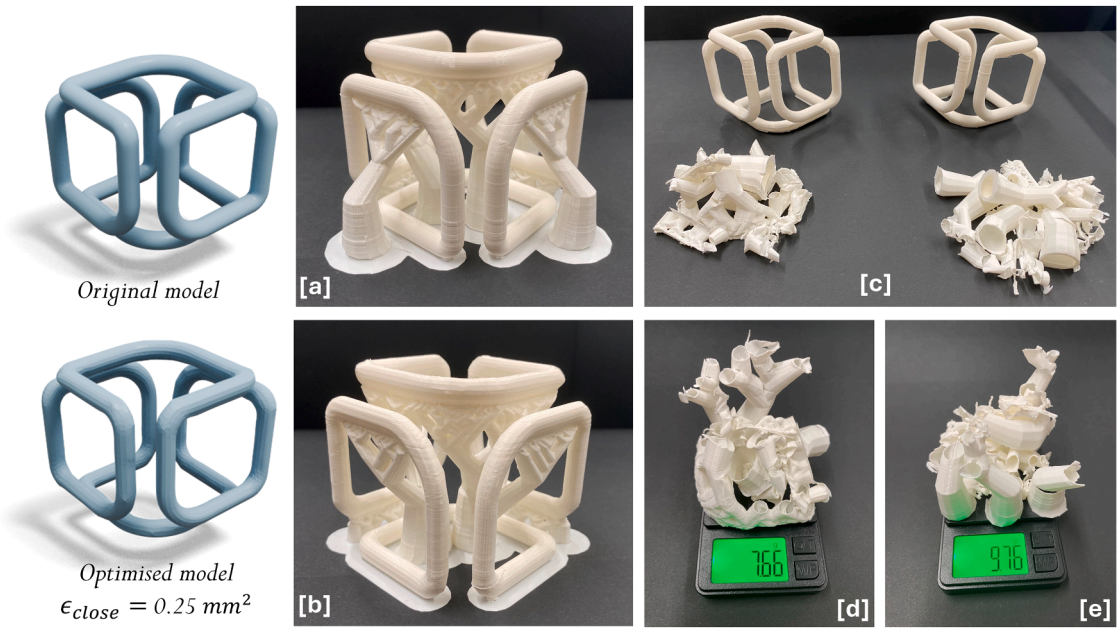

Fig. 18. Results for the Cube model (geometry-only optimisation): (a). Printed original model; (b). Printed optimised model; (c). Support removed optimised (left) and original (right) models; (d). Support structure weight of the optimised model; (e). Support structure weight of the original model.

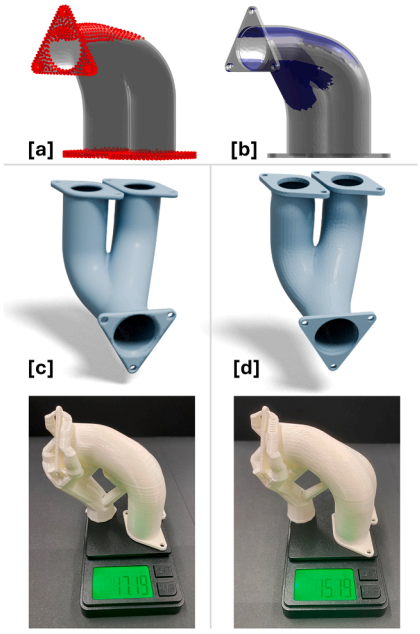

Fig. 19. Results of the Exhaust pipe model (geometry-only optimisation): (a). Fixed critical and functional regions (red); (b). Overhang regions (blue) which cause internal and external support structures; (c). Original model (top) and the total weight of the printed model (bottom); (d). Optimised model with $\epsilon_{close} = 0.1mm^2$ (top) and the total weight of the printed model (down).

addition, integrating more constraints such as symmetry and shape diameter (i.e., thickness) into our geometric optimisation can be of great importance for manufacturing-oriented design applications, which we leave as future work.

5.4.2. Towards simultaneous optimisation and integrating performance constraints

An important direction for future work is the simultaneous optimisation of part geometry and orientation to minimise support structures. Notably, simultaneous optimisation of topology and build direction for support structure minimisation has been explored in topology optimisation [38–40], where the design space is represented as a 3D density field (i.e., a volumetric representation) [40] for 3D geometries. Although our design space (i.e., vertex coordinates of boundary surface) and optimisation technique fundamentally differ from the work of Wang et al. [40], incorporating similar differentiable overhang penalties with respect to both orientation and geometry can offer strong potential to extend our alternating optimisation approach towards true simultaneous optimisation.

Although the scope of this work is limited to manufacturability improvement (i.e., support reduction), incorporating physical performance (e.g., mechanical strength) would be a crucial step to enhance the effectiveness of the current method for functional parts. While it may be challenging to formulate a generalisable integration of different performance constraints within the current framework, an interesting direction for future work would be to explore a subspace projection-based method, similar to the work proposed by Musialski et al. [15], in combination with the presented framework to enable geometric optimisation with respect to performance goals.

5.4.3. Approximation and optimisation of support structure geometry

Currently, our support structure volume proxy function achieves efficient and considerably accurate approximation of 'normal' type support column geometry. In some cases, this method can cause overestimation of the support volume compared to the ray-based method (see Fig. 3), which is non-differentiable and computationally expensive. Future work can focus on integrating differentiable methods for approximating other types of support structures (e.g., tree type [4]), and distinguishing between support columns built on the mesh surface and the build plate similar to the ray-based approach [26], to gain more accurate results. Next, although support structure geometry optimisation [4][5] is out of the scope of this work, it is strongly linked to DfAM-based shape optimisation workflows. For instance, formulating the correspondence of support structure geometry and the optimised part geometry of our iterative optimisation framework can pave new ways to realise further reduction of support structure volume.

5.4.4. Applicability of our framework to other additive manufacturing techniques

Our computational and physical printing experiments demonstrate the potential of the presented framework in improving manufacturing efficiency and reducing production costs. Although the current physical printing experiments are limited to single-material extrusion-based AM, we are confident that our optimisation framework is applicable to other AM techniques. For example, the optimised gyroid structures (see Fig. 13) can be crucial to reduce post-processing costs and waste in metal additive manufacturing applications. Therefore, further printing experiments with more AM techniques including Powder Bed Fusion (PBF), would be an important future step to validate the effectiveness and impact of the proposed optimisation framework towards high-value part manufacturing.

6. Conclusion

This paper introduces a novel mathematical framework for alternating optimisation of part orientation and geometry to reduce support structure volume in material extrusion-based 3D printing. Whilst part orientation serves as a global mechanism for support structure reduction, the proposed energy minimisation-based local geometric optimisation phase enables further reduction of support structure volume whilst minimising deviation from the original geometry and adhering to a set of geometric constraints related to manufacturing-oriented design.

The framework effectively handles models with complex geometric and topological features. For applications where orientation changes are impractical, the proposed projection-based geometric optimisation can operate independently as a standalone technique. Extensive computational and physical printing experiments using multiple FDM 3D printers, slicing software, and support structure types validate the effectiveness of the proposed framework. By demonstrating successful and efficient optimisation of a diverse range of parts, including topologically non-trivial geometries such as gyroid structures, the proposed method demonstrates its capability to significantly reduce both print time and material waste, positioning it as a promising advancement in manufacturing-oriented design.

Acknowledgements

This work has been funded by the Engineering and Physical Sciences Research Council, UK Ph.D. Studentship EP/S02297X/1. We thank Mark Dennis (School of Physics and Astronomy, University of Birmingham) for helpful comments on this work and providing continuous support.

3D model courtesy: Kitten Model – AIM Shape Repository; Armadillo – Standford 3D scanning repository; Spot – Keenan's 3D model library [41]; Cube, Knot – Cults3D model library; Exhaust pipe – Thingiverse model library.

CRediT authorship contribution statement

Don Pubudu Vishwana Joseph Jayakody: Writing – review & editing, Writing – original draft, Visualization, Validation, Software, Methodology, Investigation, Conceptualization. **Bailin Deng:** Writing – review & editing, Supervision, Methodology, Conceptualization. **Ravindra S. Goonetilleke:** Writing – review & editing, Conceptualization. **Lauren E.J. Thomas-Seale:** Writing – review & editing, Supervision, Conceptualization. **Hyunyoung Kim:** Writing – review & editing, Supervision, Resources, Conceptualization.

Declaration of competing interest

The authors declare that they have no known competing financial interests or personal relationships that could have appeared to influence the work reported in this paper.

Supplementary materials

Supplementary material associated with this article can be found, in the online version, at doi:10.1016/j.cad.2025.104029.

Data availability

Data will be made available on request.

References

[1] Gibson I, Rosen D, Stucker B, Khorasani M. Additive manufacturing technologies. Springer; 2020. https://doi.org/10.1007/978-3-030-56127-7.
[2] Zhang X, Le X, Panotopoulou A, Whiting E, Wang CCL. Perceptual models of preference in 3D printing direction. ACM Trans Graph 2015;34:1–12. https://doi.org/10.1145/2816795.2818121.
[3] C. Schranz, Tweaker-auto rotation module for FDM 3D printing, (2016). https://doi.org/10.13140/RG.2.2.27593.36966.
[4] Vanek J, Galicia JAG, Benes B. Clever support: efficient support structure generation for digital fabrication. Eurographics Symp Geom Process 2014;33:117–25. https://doi.org/10.1111/cgf.12437.
[5] Jiang J, Xu X, Stringer J. Optimization of process planning for reducing material waste in extrusion based additive manufacturing. Robot Comput Integr Manuf 2019;59:317–25. https://doi.org/10.1016/j.rcim.2019.05.007.
[6] Margadji C, Brion DAJ, Pattinson SW. Iterative learning for efficient additive mass production. Addit Manuf 2024;89:104271. https://doi.org/10.1016/j.addma.2024.104271.
[7] Hu K, Jin S, Wang CCL. Support slimming for single material based additive manufacturing. CAD Comput Aided Des 2015;65:1–10. https://doi.org/10.1016/j.cad.2015.03.001.
[8] Stava O, Vanek J, Benes B, Carr N, Měch R. Stress relief: improving structural strength of 3D printable objects. ACM Trans Graph 2012;31. https://doi.org/10.1145/2185520.2185544.
[9] Lu L, Sharf A, Zhao H, Wei Y, Fan Q, Chen X, Savoye Y, Tu C, Cohen-Or D, Chen B. Build-to-last: strength to weight 3D printed objects. ACM Trans Graph 2014;33:1–10. https://doi.org/10.1145/2601097.2601168.
[10] Wu J, Aage N, Westermann R, Sigmund O. Infill optimization for additive manufacturing-approaching bone-like porous structures. IEEE Trans Vis Comput Graph 2018;24:1127–40. https://doi.org/10.1109/TVCG.2017.2655523.
[11] Schumacher C, Bickel B, Rys J, Marschner S, Daraio C, Gross M. Microstructures to control elasticity in 3D printing. ACM Trans Graph 2015;34:1–13. https://doi.org/10.1145/2766926.
[12] Martínez J, Dumas J, Lefebvre S. Procedural voronoi foams for additive manufacturing. ACM Trans Graph 2016;35. https://doi.org/10.1145/2897824.2925922.
[13] Wang W, Wang TY, Yang Z, Liu L, Tong X, Tong W, Deng J, Chen F, Liu X. Cost-effective printing of 3D objects with skin-frame structures. ACM Trans Graph 2013;32:1–10. https://doi.org/10.1145/2508363.2508382.
[14] Zhou Y, Kalogerakis E, Wang R, Grosse IR. Direct shape optimization for strengthening 3D printable objects. Comput Graph Forum 2016;35:333–42. https://doi.org/10.1111/cgf.13030.
[15] Musialski P, Hafner C, Rist F, Birsak M, Wimmer M, Kobbelt L. Non-linear shape optimization using local subspace projections. ACM Trans Graph 2016;35:1–13. https://doi.org/10.1145/2897824.2925886.
[16] Prévost R, Whiting E, Lefebvre S, Sorkine-Hornung O. Make it stand: balancing shapes for 3D fabrication. ACM Trans Graph 2013;32:1–10. https://doi.org/10.1145/2461912.2461957.
[17] Zhang L, Wang S, Li B, Wang Y, Luo Z, Liu L. Function representation based analytic shape hollowing optimization. CAD Comput Aided Des 2022;144:103156. https://doi.org/10.1016/j.cad.2021.103156.
[18] Bächer M, Whiting E, Bickel B, Sorkine-Hornung O. Spin-it: optimizing moment of inertia for spinnable objects. ACM Trans Graph 2014;33. https://doi.org/10.1145/2601097.2601157.
[19] Jaiswal P, Rai R. A geometric reasoning approach for additive manufacturing print quality assessment and automated model correction. CAD Comput Aided Des 2019;109:1–11. https://doi.org/10.1016/j.cad.2018.12.001.
[20] Qin Y, Qi Q, Shi P, Scott PJ, Jiang X. Status, issues, and future of computer-aided part orientation for additive manufacturing. Int J Adv Manuf Technol 2021;115:1295–328. https://doi.org/10.1007/s00170-021-06996-6.
[21] Ulu E, Korkmaz E, Yay K, Burak Ozdoganlar O, Kara LBurak. Enhancing the structural performance of additively manufactured objects through build orientation optimization. J Mech Des 2015;137. https://doi.org/10.1115/1.4030998.
[22] Umetani N, Schmidt R. Cross-sectional structural analysis for 3D printing optimization, SIGGRAPH Asia 2013 Tech. Briefs, SA 2013;2013. https://doi.org/10.1145/2542355.2542361.
[23] Wang W, Shao H, Liu X, Yin B. Printing direction optimization through slice number and support minimization. IEEE Access 2020;8:75646–55. https://doi.org/10.1109/ACCESS.2020.2980282.
[24] Shi P, Qi Q, Qin Y, Meng F, Lou S, Scott PJ, Jiang X. Learn to rotate: part orientation for reducing support volume via generalizable reinforcement learning. IEEE Trans Ind Informatics 2023;19:11687–700. https://doi.org/10.1109/TII.2023.3249751.

[25] Fu H, Cohen-Or D, Dror G, Sheffer A. Upright orientation of man-made objects. SIGGRAPH'08 Int Conf Comput Graph Interact Tech 2008;1. https://doi.org/10.1145/1399504.1360641. ACM SIGGRAPH 2008 Pap. 2008.
[26] Allaire G, Bihr M, Bogosel B. Support optimization in additive manufacturing for geometric and thermo-mechanical constraints. Struct Multidiscip Optim 2020;61:2377–99. https://doi.org/10.1007/s00158-020-02551-1.
[27] Filoscia I, Alderighi T, Giorgi D, Malomo L, Callieri M, Cignoni P. Optimizing Object decomposition to reduce visual artifacts in 3D printing. Comput Graph Forum 2020;39:423–34. https://doi.org/10.1111/cgf.13941.
[28] Niesen U, Shah D, Wornell GW. Adaptive alternating minimization algorithms. IEEE Trans Inf Theory 2009;55:1423–9. https://doi.org/10.1109/TIT.2008.2011442.
[29] Hannay JH, Nye JF. Fibonacci numerical integration on a sphere. J Phys A Math Gen 2004;37:11591–601. https://doi.org/10.1088/0305-4470/37/48/005.
[30] Taubin G. Curve and surface smoothing without shrinkage. IEEE Int Conf Comput Vis 1995:852–7. https://doi.org/10.1109/iccv.1995.466848.
[31] Bouaziz S, Deuss M, Schwartzburg Y, Weise T, Pauly M. Shape-up: shaping discrete geometry with projections. Eurographics Symp Geom Process 2012;31:1657–67. https://doi.org/10.1111/j.1467-8659.2012.03171.x.
[32] Horn BKP. Closed-form solution of absolute orientation using unit quaternions. J Opt Soc Am A 1987;4:629. https://doi.org/10.1364/josaa.4.000629.
[33] Lee CH, Varshney A, Jacobs DW. Mesh saliency. ACM Trans Graph 2005;24:659–66. https://doi.org/10.1145/1073204.1073244.
[34] Mittal Y, Agarwal V, Yadav D, Avegnon KL, Sealy M, Kamble P, Gote G, Patil Y, Mehta A, Mandal P, Karunakaran KP. A mechanistic model for overhang limits in additive manufacturing. Prog Addit Manuf 2025. https://doi.org/10.1007/s40964-025-01154-w.
[35] Nealen A, Igarashi T, Sorkine O, Alexa M. Laplacian mesh optimization. In: Proc. - Graph. 2006 4th Int. Conf. Comput. Graph. Interact. Tech. Australas.; 2006. p. 381–9. https://doi.org/10.1145/1174429.1174494.
[36] Zhang JE, Jacobson A, Alexa M. Fast updates for least-squares rotational alignment. Comput Graph Forum 2021;40:13–22. https://doi.org/10.1111/cgf.142611.
[37] Peng Y, Deng B, Zhang J, Geng F, Qin W, Liu L. Anderson acceleration for geometry optimization and physics simulation. ACM Trans Graph 2018;37. https://doi.org/10.1145/3197517.3201290.
[38] Langelaar M. Combined optimization of part topology, support structure layout and build orientation for additive manufacturing. Struct Multidiscip Optim 2018;57:1985–2004. https://doi.org/10.1007/s00158-017-1877-z.
[39] Jiang J, Xu X, Stringer J. Support structures for additive manufacturing: A review. J Manuf Mater Process 2018;2. https://doi.org/10.3390/jmmp2040064.
[40] Wang C, Qian X. Simultaneous optimization of build orientation and topology for additive manufacturing. Addit Manuf 2020;34:101246. https://doi.org/10.1016/j.addma.2020.101246.
[41] K. Crane, Keenan's 3D model repository, 2022. Available: https://www.cs.cmu.edu/kmcrane/Projects/ModelRepository/.